AGU PUBLICATIONS

Paleoceanography

RESEARCH ARTICLE
10.1002/2014PA002640

Andean elevation control on tropical Pacific climate and ENSO

Ran Feng[1] and Christopher J. Poulsen[1]

[1]Department of Earth and Environmental Sciences, University of Michigan, Ann Arbor, Michigan, USA

Key Points:
- CCSM4 is used to study responses of tropical Pacific climate to Andean uplift
- Andean uplift invokes a La Niña-like SST response
- Andean uplift reduces the ENSO frequency and strong El Niño events

Correspondence to:
R. Feng,
rfeng@umich.edu

Citation:
Feng, R., and C. J. Poulsen (2014), Andean elevation control on tropical Pacific climate and ENSO, *Paleoceanography*, *29*, 795–809, doi:10.1002/2014PA002640.

Received 11 MAR 2014
Accepted 15 JUL 2014
Accepted article online 18 JUL 2014
Published online 11 AUG 2014

Abstract Late Cenozoic marine proxy data record a long-term transition in the tropical Pacific from El Niño-like conditions with reduced zonal sea surface temperature (SST) gradient, deepened thermocline, and reduced upwelling in the eastern equatorial Pacific (EEP) to conditions similar to modern. This transition coincides with kilometer-scale uplift of the central Andes. To understand whether the rise of the Andes contributed to tropical Pacific climate evolution, we performed experiments with the National Center for Atmospheric Research's Community Climate System Model version 4 to quantify changes in tropical Pacific climate and El Niño–Southern Oscillation as a function of Andean elevations. Our results demonstrate that uplift increases the equatorial east-west SST gradient and Walker circulation. The rise of the Andes from 1 to 3 km increases the SST gradient by 0.8°C and Walker circulation by 60% due to strengthened radiative cooling by enhanced low-cloud formation in the EEP. This cooling effect is largest in the southeastern tropical Pacific and accounts for about one half of the reconstructed SST cooling along the Peru coast. The uplift also strengthens upwelling north of the EEP, consistent with documented increases in biological productivity in this region, and decreases the frequency of El Niño–Southern Oscillation and the number of strong El Niño events. Simulated responses to Andean uplift are generally consistent with the late Cenozoic proxy records, but too small in magnitude. Taken together, our results indicate that Andean uplift was likely one of the multiple factors that contributed to the long-term evolution of both the mean climate state and the interannual variability in the tropical Pacific.

1. Introduction

Geological evidence suggests that the tropical Pacific climate evolved through the late Cenozoic from a mean state with a reduced zonal sea surface temperature (SST) gradient across the equatorial Pacific to its current state [*Wara et al.*, 2005; *Fedorov et al.*, 2006; *Zhang et al.*, 2014]. In comparison to today, the western equatorial Pacific during the early Pliocene (~5 Ma) had similar SSTs [*Wara et al.*, 2005]; however, the eastern equatorial Pacific (EEP) was characterized by SSTs that were ~2 to 6°C warmer [*Wara et al.*, 2005; *Lawrence et al.*, 2006; *Steph et al.*, 2010; *Dekens et al.*, 2007], a deeper thermocline [*Wara et al.*, 2005; *Lawrence et al.*, 2006; *Steph et al.*, 2010], and lower biologic productivity and richness [*Wara et al.*, 2005; *Dekens et al.*, 2007; *Lawrence et al.*, 2006; *Kamikuri et al.*, 2009; *Steph et al.*, 2010].

These proxy observations were originally used as evidence for a "permanent El Niño" state with a negligible zonal SST gradient across the equatorial Pacific [*Wara et al.*, 2005; *Fedorov et al.*, 2006], which was thought to have ended with intensification of the EEP cold tongue at ~3 Ma [*Wara et al.*, 2005] or ~4 Ma [*Lawrence et al.*, 2006; *Steph et al.*, 2010]. This argument is consistent with the early Pliocene terrestrial records of temperature and precipitation from around the world, which have been suggested to exhibit far-field patterns similar to those that occur during modern El Niño events [*Molnar and Cane*, 2007], although different causes such as changes in the early Pliocene surface conditions and CO_2 levels could also produce these patterns [*Bonham et al.*, 2009]. More recent studies of marine sediment cores that extend into the Miocene challenge the suggested permanent El Niño state [*Nathan and Leckie*, 2009; *Zhang et al.*, 2014]. New SST estimates suggest that an SST zonal gradient of ~3°C was sustained through the late Miocene and increased during the Plio-Pleistocene [*Zhang et al.*, 2014]. And, records of marine production indicate that upwelling in the northern EEP (6°N, 86°W) began to intensify in the late Miocene (13 Ma), suggesting that the transition to modern conditions may have started much earlier than the Pliocene [*Kamikuri et al.*, 2009; *LaRiviere et al.*, 2012]. Although the late Cenozoic marine records differ in detail, they generally record a strengthening of the climate asymmetry in the tropical Pacific. The cause of this transition is crucial to understanding the formation and stability of modern climate variability.

The evolution of the tropical Pacific has been linked to both long-term changes in CO_2 levels and episodic gateway changes in the late Cenozoic. However, none of these mechanisms can explain the changes documented in marine proxy records. CO_2-induced cooling has been found to have little direct effect on the SST gradient across the tropical Pacific [e.g., *Lee and Poulsen*, 2006; *Haywood et al*., 2007; *Fedorov et al*., 2013]. The widening of the Indonesian Seaway increases warm and freshwater flow to the central equatorial Pacific, which decreases the frequency of the El Niño–Southern Oscillation (ENSO), but has little influence on simulated SSTs in the eastern Pacific [*Jochum et al*., 2009]. And, finally, the closing of the Panama Seaway raises the EEP thermocline by reducing the flow of warm waters from the western Atlantic [*Steph et al*., 2010; *Zhang et al*., 2010]; however, the SST response is quite small in coupled experiments and has little effect on the zonal gradient across the equatorial Pacific [*Zhang et al*., 2010; *Fedorov et al*., 2013]. Besides, the closing of the Panama Seaway remains controversial. Closure ages are proposed to be between 4 and 5 Ma based on ocean drilling records [*Haug and Tiedemann*, 1998] or at ~15 Ma based on geological mapping and geochronological and geochemical data from central Panama [*Montes et al*., 2012].

Other mechanisms have been proposed to explain the evolution of the tropical Pacific including an enhanced tropical-extratropical thermogradient [*Fedorov et al*., 2006; *Brierley et al*., 2009], expansion of Southern Ocean sea ice [*Lee and Poulsen*, 2006], and decrease in the frequency of tropical storms [*Fedorov et al*., 2010]. Mechanisms such as dwindling CO_2 level, expansion of sea ice, or decreasing albedo of the extratropical low clouds [*Fedorov et al*., 2013] are needed to explain the enhanced thermogradient. Therefore, unlike the other two, the thermogradient hypothesis by itself should not be considered as a direct forcing. Climate modeling studies of sea ice expansion and decreasing frequency of tropical storms show reasonable agreement with proxy observations. An increase in Southern Ocean sea ice from ice free to modern extents in a coupled ocean-atmosphere model enhanced cold-water advection into the EEP through the meridional thermocline circulation, leading to an ~2°C decrease in SSTs in the EEP. Similarly, a decrease in ocean diffusivity (by 10 times), representing weakened mixing due to reduced frequency of tropical storms, in another coupled model cooled SSTs in the EEP by 2.5°C [*Fedorov et al*., 2010]. Both mechanisms produce cooling that is consistent with proxy records, but until compelling geological evidence is found for either mechanism, both must be considered to be somewhat ad hoc.

A significant surface uplift of the Andes due to subduction of the Nazca plate beneath South America occurred since the late Miocene (see summary by *Insel et al*. [2012]). The possibility that Andean surface uplift influenced tropical Pacific climate draws support from dynamical studies. Notably, *Rodwell and Hoskins* [2001] found using a simplified atmospheric model that a high-elevation Andes strengthened the southeastern Pacific subtropical high-pressure system. Because the subtropical high is a dynamic response to subsidence of dry air, the intensification of the high was speculated to coincide with evaporative cooling of the sea surface. *Takahashi and Battisti* [2007a], using a simplified atmospheric model with a mixed-layer ocean, confirmed this linkage. In addition, they found that enhanced low-cloud formation in the southeastern tropical Pacific (SETP) contributed to SST cooling as well. Together these factors lead to a total cooling of up to 4°C. The application of these studies to the late Cenozoic is limited, however by their idealized nature and the absence of dynamic ocean-atmosphere interactions. In this study, we use an Earth system model with coupled ocean-atmosphere dynamics to overcome this limitation.

The details and timing of Andean uplift are uncertain. Terrestrial proxy data from the Andean Altiplano have been argued to record rapid surface uplift of the central Andes by 2.5 ± 1 km between 10 Ma and 6 Ma [*Garzione et al*., 2008; *Ghosh et al*., 2006; *Leier et al*., 2013] that proceeded from south to north [*Gregory-Wodzicki*, 2000]. This interpretation of a rapid rise has been disputed in favor of more gradual uplift through the Cenozoic [e.g., *Ehlers and Poulsen*, 2009; *Poulsen et al*., 2010; *Insel et al*., 2012]. Nonetheless, most geological studies support uplift of approximately 2 km since 15 Ma (see summary by *Insel et al*. [2012]), which coincides with the long-term increase in upwelling and SST cooling documented in the northern and western EEP. Due to uncertainties in both timing and distribution of surface uplift, we do not assign any particular ages to our simulations. Previous studies [*Lenters and Cook*, 1997; *Insel et al*., 2010] have investigated the influence of Andean surface uplift on the large-scale dynamics over the continent. Here we focus on the role of the Andes in setting conditions over the tropical Pacific region.

In addition to the mean state, we also explore whether Andean uplift alters interannual variability (ENSO) in the tropical Pacific. High-resolution sedimentary records of late Miocene and early Pliocene ages from the equatorial Pacific [*Scroxton et al*., 2011; *Watanabe et al*., 2012] and Mediterranean region [*Galeotti et al*., 2010] contain sedimentary features that are thought to represent ENSO variability, indicating that even under a

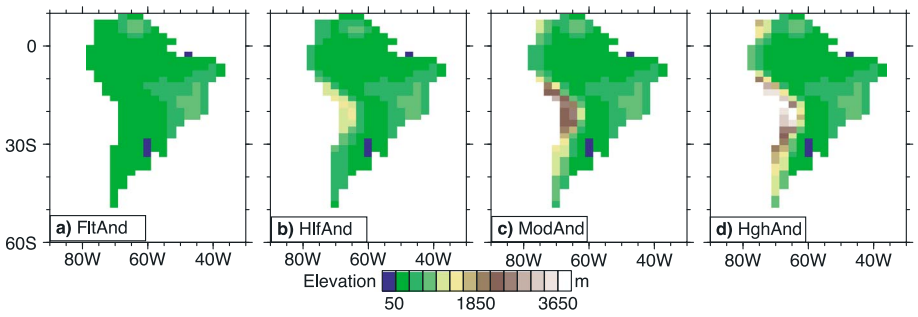

Figure 1. South American elevations specified in the (a) FltAnd, (b) HlfAnd, (c) ModAnd, and (d) HghAnd experiments. The ModAnd features the standard topography of CCSM4, in which the elevation is averaged within each 2° grid cell yielding average elevations in the central Andes of ~2 km. The elevations of the central Andes are ~145 m and ~1 km in the FltAnd and HlfAnd and increase to ~3 km in the HghAnd.

climatological state with low equatorial SST gradient, the ENSO cycle was active in the early Pliocene. However, whether the strength and frequency of ENSO are different from modern is unclear but crucial to understanding past climate variability. In this study, we show based on our modeling results a connection between the ENSO and the Andean uplift.

2. Methods

The Community Climate System Model version 4 (CCSM4) [*Gent et al*., 2011] is configured to include the Community Atmospheric Model version 4 (CAM4), a dynamical ocean model of Parallel Ocean Program version 2 (POP2), Community Land Model version 4 (CLM4), and the Los Alamos Sea Ice model. All components are coupled through the version 7 coupler. Both CAM4 and CLM4 are run at 1.9°×2.5° horizontal resolution; CAM4 has 26 vertical levels. POP2 is configured with a 384 × 320 horizontal grid, 60 vertical layers, and a rotated north pole centered on Greenland. Preindustrial boundary conditions are prescribed, including a CO_2 level of 287.4 ppm, a solar constant at 1360.9 W/m^2, and preindustrial vegetation distribution and land surface types (see details in *Gent et al*. [2011]).

Four topographic scenarios are prescribed in CAM4 (Figures 1a–1d) with gradual rise of the entire South American coastal range, the elevation of which is adjusted proportionally to preserve its modern horizontal extent. The horizontal extent of the Andes, which has previously been shown to have no significant effect on the topography-induced dynamics [*Takahashi and Battisti*, 2007b], is kept the same for all experiments. The Altiplano region is raised incrementally from approximately sea level (145 m, averaged across 16–23°S, 70–65°W) (referred to as "FltAnd") to a moderate height of 1059 m (referred to as "HlfAnd"), a standard height in CCSM4 of 2272 m (referred to as "ModAnd"), and a higher elevation of 3184 m (referred to as "HghAnd") comparable to the averaged elevation across the entire modern Altiplano (3365 m calculated from GTOPO30 data (http://webgis.wr.usgs.gov/globalgis/gtopo30/gtopo30.html at 10 min resolution). It should be noted that the default prescription of the Andes in a 2 × 2° CCSM4 modern simulation is lower than observation due to grid-scale averaging of topography (Figure 1c). Land surface boundary conditions are unchanged across experiments, eliminating the response of vegetation and land surface hydrology to elevation changes. All four experiments are branched from the end of a 1000 year preindustrial control experiment and integrated for another 300 years. The diagnostics for the control experiment can be found at http://www.cesm.ucar.edu/experiments/cesm1.0/.

CCSM4 simulates SST in the EEP reasonably well. SSTs adjacent to the northern Chilean coast are too warm by 1–2°C due to coastal southerly winds that are too weak in the 2° grid configuration. A 0.5° grid simulation with the same physics packages but refined topography forces stronger southerly wind stress that eliminates this bias, indicating that the model physics is not the primary culprit [*Gent et al*., 2009]. Higher-resolution experiments may better constrain the exact magnitude of climate responses to the Andean uplift but are not expected to change fundamentally with the same model physics. The simulated ENSO amplitude in CCSM4 is overestimated by 70% in a 2 × 2° modern simulation and has a stronger than normal 4 year power spectrum peak [*Deser et al*., 2012]. Nonetheless, CCSM4's ENSO simulation is among the best of the newest generation of coupled models, and its 4 year cycle falls within modern observations [*Bellenger et al*., 2013].

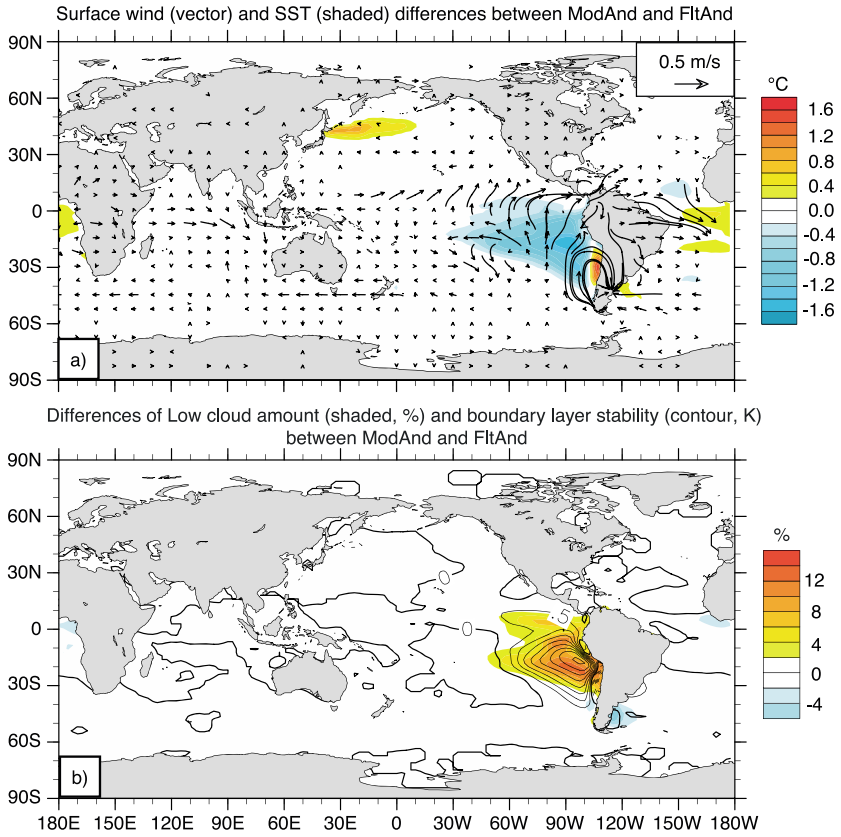

Figure 2. Global responses of SST and low-level atmosphere to the Andean uplift from FltAnd to ModAnd. (a) Mean SST (°C, shaded) and surface wind (m/s, vectors) differences. (b) Differences of low-cloud fraction (%, shaded) and marine boundary layer stability (*K*, contour). The marine boundary layer stability is measured by taking the difference of equivalent potential temperature between 700 hPa and 1000 hPa. Only responses that have passed consistency tests are shown.

The Niño 3.4 index is used here to identify the frequency of ENSO. The index is defined as the 5 month running mean of the departure in monthly SST from its 30 year average across the central equatorial Pacific (170°W–120°W, 5°N–5°S). Modern El Niño events are identified as periods when the Niño 3.4 is equal to or greater than 0.4°C for a minimum duration of 5 months [*Trenberth*, 1997]. In modeling studies, the criteria for identifying El Niño events are somewhat different to account for systematic model biases. In CCSM, the standard deviation (σ) of the Niño 3.4 ($\sigma_{\text{Niño 3.4}}$) across climatological time scales has been used to identify El Niño and La Niña [*Deser et al*., 2012; *Bellenger et al*., 2013]. In our experiments, the probability density functions of the monthly Niño 3.4 of the last 230 year experiments form a single distribution that is close to normal, implying no systematic shifts of the Niño 3.4 statistics across different climatological time scales. Thus, following *Bellenger et al*. [2013], the $\sigma_{\text{Niño 3.4}}$ of the entire 230 year time series is used to identify the El Niño and La Niña events. We define El Niño (La Niña) events as having a Niño 3.4 greater (smaller) than 0.5 $\sigma_{\text{Niño 3.4}}$ ($-0.5\,\sigma_{\text{Niño 3.4}}$) for at least 5 months. A value of 0.5 $\sigma_{\text{Niño 3.4}}$ is equivalent to a Niño 3.4 amplitude of 0.7°C from modern SST observations, which is higher than the threshold of 0.4°C used to identify El Niño and La Niña events from observations. This threshold choice minimizes the bias in CCSM 4 to overestimate Niño 3.4 variations.

The upper layer ocean equilibrates during the first 70 years in all the four branched experiments. Upper layer (0–500 m) seawater trends in the following 230 years are less than 0.01°C/century over the entire ocean and less than 0.06°C/century in the EEP region (5°S–5°N, 90°W–120°W). The global mean upper layer seawater temperature is similar (~11.3°C) in all the four experiments. Climate responses are reported here as differences from the FltAnd case and are based on results from the last 230 years of simulation. In section 3, we focus on comparisons between the ModAnd and FltAnd experiments for brevity; differences between the HghAnd and FltAnd experiments are similar though slightly larger in magnitude.

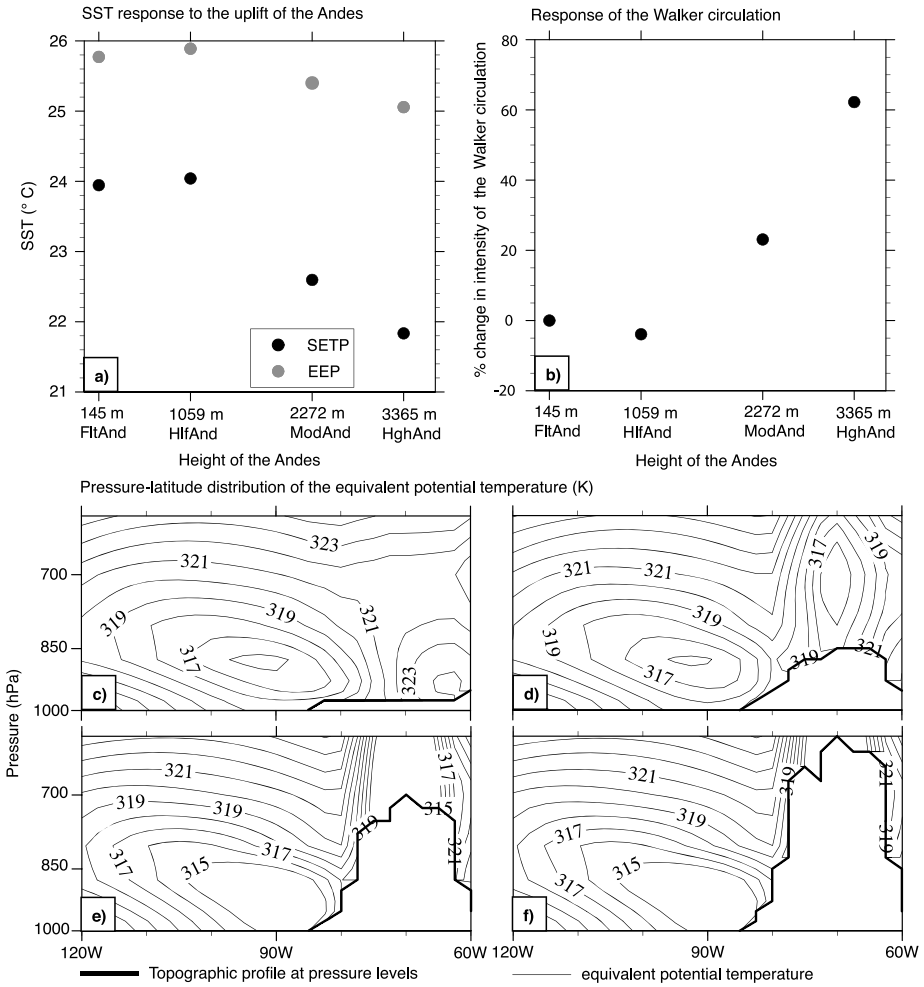

Figure 3. Climatological responses to the rise of Andes. (a) Mean SST in the southeastern tropical Pacific and the eastern equatorial Pacific. (b) Changes in intensity (%) of the Walker circulation. (c and f) Zonal profile of equivalent potential temperature (K) averaged over 10–20°S of difference stages of Andean uplift (c: FltAnd; d: HlfAnd; e: ModAnd; f: HghAnd). The strength of Walker circulation is measured by the sea level pressure difference between the western (5°S–5°N, 80°E−160°E) and eastern (5°S–5°N, 160°W−80°W) equatorial Pacific.

In order to retain the responses mostly due to changes in the mean state, we perform a consistency test when analyzing the climate responses to surface uplift (Figures 3, 6, and 7b). Consider a multidecadal oscillation with the same period and average amplitude. A phase offset between experiments could result in net differences if the averaging time is not exactly one or a multiple of periods. Similar differences could also result from temporal variations in oscillation amplitudes. These differences, if measured at decadal time scales, may vary in sign, while differences in background states should be consistent. We compare the sign of differences between the mean fields calculated on 30 year time intervals (20 years for the final interval) at each grid point. Differences that vary in sign across these intervals are considered inconsistent and are not reported.

3. Results

3.1. La Niña-Like SST Response to the Uplift of the Andes

The strongest SST responses to Andean uplift occur in the EEP and SETP. SST responses are small outside the tropical Pacific. Moderate warming in the northwestern Pacific and tropical Atlantic (Figure 2a) is reminiscent of extratropical SST responses to the La Niña-like tropical conditions [e.g., *Alexander et al*., 2002].

The responses of tropical climate to Andean uplift are nonlinear (Figures 3a and 3b) with notable changes in SST and zonal circulation occurring when the range exceeds the marine boundary layer of the eastern tropical Pacific,

Table 1. Differences (ModAnd − FltAnd) of Individual Forcing Averaged Over the Eastern Equatorial Pacific (EEP) (5°S–5°N, 90°–130°W) and the Southeastern Tropical Pacific (SETP) (15°S–20°S, 80°W–100°W) Due to Surface Uplift

	Boundary Layer Stability	Latent Heat Flux	Temperature Change (ΔT) Due to Low-Level Horizontal Advection	ΔT (700 hPa) Due to Vertical Advection	Shortwave Cloud Forcing	Longwave Cloud Forcing
EEP	+0.7°C	−0.1 W/m^2	−0.1°C/day	0°C/day	−8.5 W/m^2	−0.1 W/m^2
SETP	+3.5°C	−0.2 W/m^2	−0.6°C/day	+0.8°C/day	−1.8 W/m^2	−1.3 W/m^2

a height of more than 1100 m [*Wood and Bretherton*, 2004]. This layer can be identified by the large vertical gradient of equivalent potential temperature [*Xu et al.*, 2004], which separates the low-level mixed layer from the upper level free troposphere. In our simulations, the top of the marine boundary layer occurs between ~860 hPa and 700 hPa with much better defined boundaries in ModAnd and HghAnd as compared to the FltAnd and HlfAnd (Figures 3c–3f).

In ModAnd and HghAnd, the uplift of the Andes above the marine boundary layer leads to SST cooling of 0.4°C and 0.8°C in the EEP and 1.5°C and 2.2°C in the southeastern tropical Pacific (SETP) (15°–20°S, 80°W–100°W) (Figure 3a). Within the equatorial zone, this nonlinear SST response is coupled with strengthening of the Walker circulation, measured as the sea level pressure difference between the western (5°S–5°N, 80°E–160°E) and eastern (5°S–5°N, 160°W–80°W) equatorial Pacific [*Vecchi and Soden*, 2007]. The strength of Walker circulation increases by 22% in ModAnd and additional 28% in HghAnd (Figure 3b). SST cooling is accompanied by anomalous surface wind divergence in the eastern tropical Pacific and strengthened easterlies at the western equatorial Pacific (120°E–180; Figure 2a). The coupling between SSTs, the Walker circulation, and the equatorial easterlies comprises a Bjerknes feedback that strengthens the zonal SST gradient and enhances La Niña-like mean conditions.

3.2. Cooling Due to Increased Low Clouds

Increases in surface latent heat loss [*Takahashi and Battisti*, 2007a] and low-cloud amounts by Andean uplift [*Xu et al.*, 2004; *Takahashi and Battisti*, 2007a] have previously been suggested as mechanisms for SST cooling in the EEP and SETP. In our ModAnd experiment, radiative cooling due to enhanced shortwave reflection by low clouds contributes the largest forcing, which is locally as much as −8.5 W/m^2 (Table 1). Low clouds are enhanced year round by a strengthened marine boundary layer with a strong inversion cap (Figure 2b and Table 1), which is a result of uplift-induced circulation changes. A high Andes blocks northeasterly flow from northern South America and steers midlatitude westerlies in the southeastern Pacific toward the equator (Figure 2a). These changes in flow pattern induce advective cooling in the lower atmosphere (1000–900 hPa) of the EEP and SETP (Table 1). At the SETP, middle tropospheric subsidence is strengthened by Andean uplift, inducing anomalous subsidence warming on top of the boundary layer (Table 1). Both advective low-level cooling and higher-level warming enhance the temperature difference across the boundary inversion, leading to a stronger moisture cap and greater low-cloud amounts.

Surface cooling at the EEP and SETP is partially attenuated by subsurface warming in the southeastern Pacific. This warming is due to the weakening of the Pacific subtropical overturning cell (STC), a wind-driven isopycnal flow that forms a meridional circulation in the upper (~200 m) tropical Pacific [*Gu*, 1997] and mixes tropical and subtropical waters through tropical thermocline upwelling of subtropical waters [*Klinger et al.*, 2002]. The STC consists of two meridional cells in the northern and southern tropical Pacific; however, only the southern STC is well defined in the eastern Pacific (Figure 4a). This southern STC extends from 150°W to 85°W at 9°S with a core at ~50 m depth. We mainly focus here on the eastern portion of the southern STC (ESSTC) from 100°W to 85°W, which underlies uplift-induced SST cooling in the SETP.

In comparison to FltAnd, the ESSTC is slower in the ModAnd experiment with reduced upward transport in the extraequatorial region (10°S–15°S) and downwelling in the southern subtropics (17°S–25°S) (Figure 4b). At 15°S, the vertical velocity of water flow is 1.4×10^{-2} cm/s in FltAnd at 285 m depth, which decreases to 0 in ModAnd. This decrease does not follow the isopycnal slant toward the equator but mainly occurs at 15°S–16°S as a result of anomalous Ekman downwelling (Figure 4c). The weakening of the ESSTC reduces equatorward transport of cooler waters from the middle latitudes, resulting in warming (up to 2°C) of the subtropical ocean below the thermocline (20°C isotherm) (Figures 4b and 4d). This anomaly propagates northward to

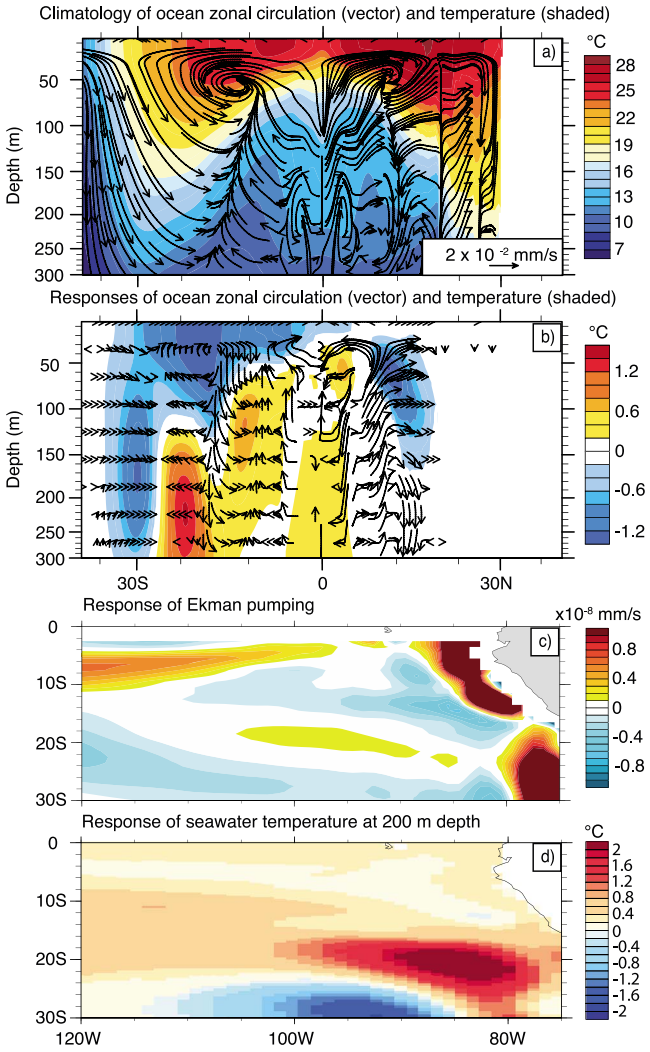

Figure 4. Ocean climatology and dynamical responses to Andean uplift in the eastern Pacific Ocean (100°W–80°W). (a) Latitude-depth profile of the mean ocean circulation (vectors, 10^{-2} mm/s) and temperature (°C) of FltAnd. (b–d) Horizontal climatological responses to the Andean uplift: (Figure 4b) Subsurface temperature (°C) and circulation (10^{-2} mm/s), (Figure 4c) surface Ekman pumping speed (10^{-8} mm/s), and (Figure 4d) 200 m seawater temperature (°C) of the southern tropical Pacific (30°S–0°S). The vertical velocity of the ocean current is exaggerated by 10^5 times for visual purpose. The Ekman pumping speed within 2°S–0°S is masked due to minimal Coriolis force around the equator.

warm the entire subsurface EEP (below 40 m). Thermocline upwelling of this anomalously warm water serves as a negative feedback that compensates surface cooling due to greater low-cloud amounts. Consistent with this result, the cooling response to Andean uplift is larger (up to 4°C compared to 2°C in our simulations) in simulations using an atmospheric model coupled to a mixed layer ocean model that does not allow for ocean dynamical adjustment [*Takahashi and Battisti*, 2007a].

3.3. ENSO Response to Andean Uplift

The ENSO response to Andean uplift is nonlinear. The ENSO response to uplift to HlfAnd is quite small. The spectral density of the Niño 3.4 index peaks at the same period as FltAnd with a slight increase in the peak density (not shown). These small responses are consistent with minimal changes in climate state of the tropical Pacific between FltAnd and HlfAnd. In contrast, in the ModAnd and HghAnd cases, the ENSO cycle lengthens in comparison to FltAnd as shown by a systematic shift in the mean spectral density of the Niño 3.4 indices to longer periods (Figure 5a).

Kirtman [1997] suggests a link between anomalies of zonal wind stress curl and the length of the ENSO cycle, in which the former generates off-equatorial Rossby waves that weaken the strength of the reflected Kelvin wave at the western boundary. This weakening of the reflected Kelvin wave reduces damping of ENSO-related equatorial SST anomalies. Our experiments are consistent with this idea. The lengthening of the ENSO cycle is accompanied by greater variability of the monthly zonal wind stress curl in the northern region of the western and central Pacific (4°N–10°N, 120°E–180°E) in ModAnd and HghAnd (Figure 5b), which feasibly favors off-equatorial Rossby waves in the north. Although uplift leads to a reduction in the variability of wind stress curl in the southern region (4°S–10°S, 120°E–180°E), the differences in magnitude are relatively small. As a result, the net changes of zonal wind stress curl favor weaker reflected Kelvin waves and more persistent SST anomalies. Lengthening of the ENSO cycle explains the slight decrease in the total number of El Niño events with Niño 3.4 ≥ 0.5 $\sigma_{\text{Niño 3.4}}$: there are 40 events in FltAnd and 36 and 39 events in ModAnd and HghAnd.

In addition to fewer events, Andean uplift also influences the magnitude distribution of El Niño events. The El Niño events shifted slightly toward the weaker magnitude side in HlfAnd (not shown). Both ModAnd and HghAnd feature a significant reduction in strong El Niño events (Figure 5c). There are fewer strong events with Niño 3.4 values between 1.0 and 2.5 $\sigma_{\text{Niño 3.4}}$ (9 fewer events in both cases) but more mild events

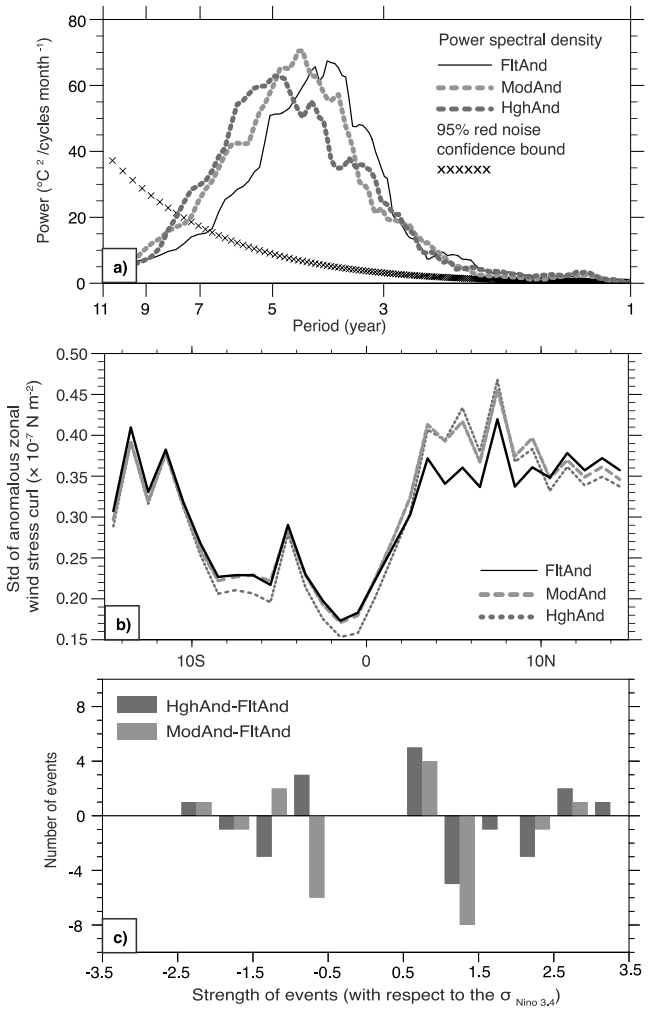

Figure 5. ENSO response to Andean uplift. (a) Spectral density of the Niño 3.4 index of the FltAnd, ModAnd, and HghAnd; (b) latitudinal distribution of standard deviation of anomalous monthly zonal wind stress curl averaged across the extraequatorial western Pacific (120°E–180°E); (c) difference from FltAnd in the number of El Niño and La Niña events in the ModAnd and HghAnd simulations. Magnitudes are binned in intervals of 0.5 $\sigma_{Niño3.4}$. In Figure 5b, the seasonal cycle is removed from the time series of anomalous monthly zonal wind stress curl. The 9 year high-pass Lanczos filter [*Duchon*, 1979] using 108 weights is applied to the Niño 3.4 index prior to the spectral analysis in Figure 5a to remove the decadal variation of the time series. The 95% red noise confidence bound is shown for FltAnd. Bounds are similar among experiments.

with values between 0.5 to 1.0 $\sigma_{Niño\ 3.4}$ (4 more events in ModAnd and 5 more in HghAnd; Figure 5c). The number of extremely warm El Niño events with Niño 3.4 values between 2.5 and 3.5 $\sigma_{Niño\ 3.4}$ increases slightly in both experiments (1 more event in ModAnd and 2 more events in HghAnd), but the increase is rather small and might be a result of internal variability independent of the Andean uplift. The response of La Niña events to uplift is less clear; there are no systematic changes in the number of weak or strong events (Figure 5a).

The reduction in the number of strong El Niño events (1.0 $\sigma_{Niño\ 3.4} \le$ Niño 3.4 $\le$ 2.5 $\sigma_{Niño\ 3.4}$) is associated with seasonal SST cooling (Figures 6a–6h) and upwelling intensification (Figures 6i–6p, indicated by the red shade) in the central and western equatorial Pacific from December to March. The emergence of SST and upwelling anomalies during December is accompanied by stronger equatorial easterly wind stress (discussed in detail below) in the central equatorial Pacific (between ~130°E and 160°W; Figure 6l). These seasonal adjustments, which can be viewed as a strengthened Bjerknes feedback, suppress SST warming and thermocline deepening in the central equatorial Pacific during the austral summer when the majority of El Niño events (>60% of all the experiments) reach the highest Niño 3.4 values.

3.4. Diabatic Response of Regional Circulation

Strengthening of the Bjerknes feedback by uplift mainly occurs during the austral summer (Figures 6d–6f and Figures 6l–6n) and coincides with the enhanced SST cooling by low clouds (Figures 6t–6v). This low-cloud cooling effect persists throughout the year but is greatest during the austral summer and extends farther west (10°S–25°S, 100°W–135°W) from December to March (Figures 6t–6w).

Enhanced low-cloud formation in the summer is a result of uplift-induced diabatic circulation over the eastern central extraequatorial Pacific. Andean uplift enhances the seasonal cycle of moist heating around the central Andes (600 hPa; 27.5°S–10°S, 83°W–58°W) (Figure 7a). (Moist heating is calculated as the product of the rate of temperature changes due to moist processes and the specific heat capacity of the moist air and includes both latent heat release during condensation and heat exchange during mixing processes associated with formation of clouds and precipitation.) The enhancement of moist heating, though persistent with elevation increase, is nonlinear and peaks between the HlfAnd and ModAnd runs. In ModAnd, the net moist heating in the summer is about twice the amount of that in FltAnd. This additional heating drives an anomalous

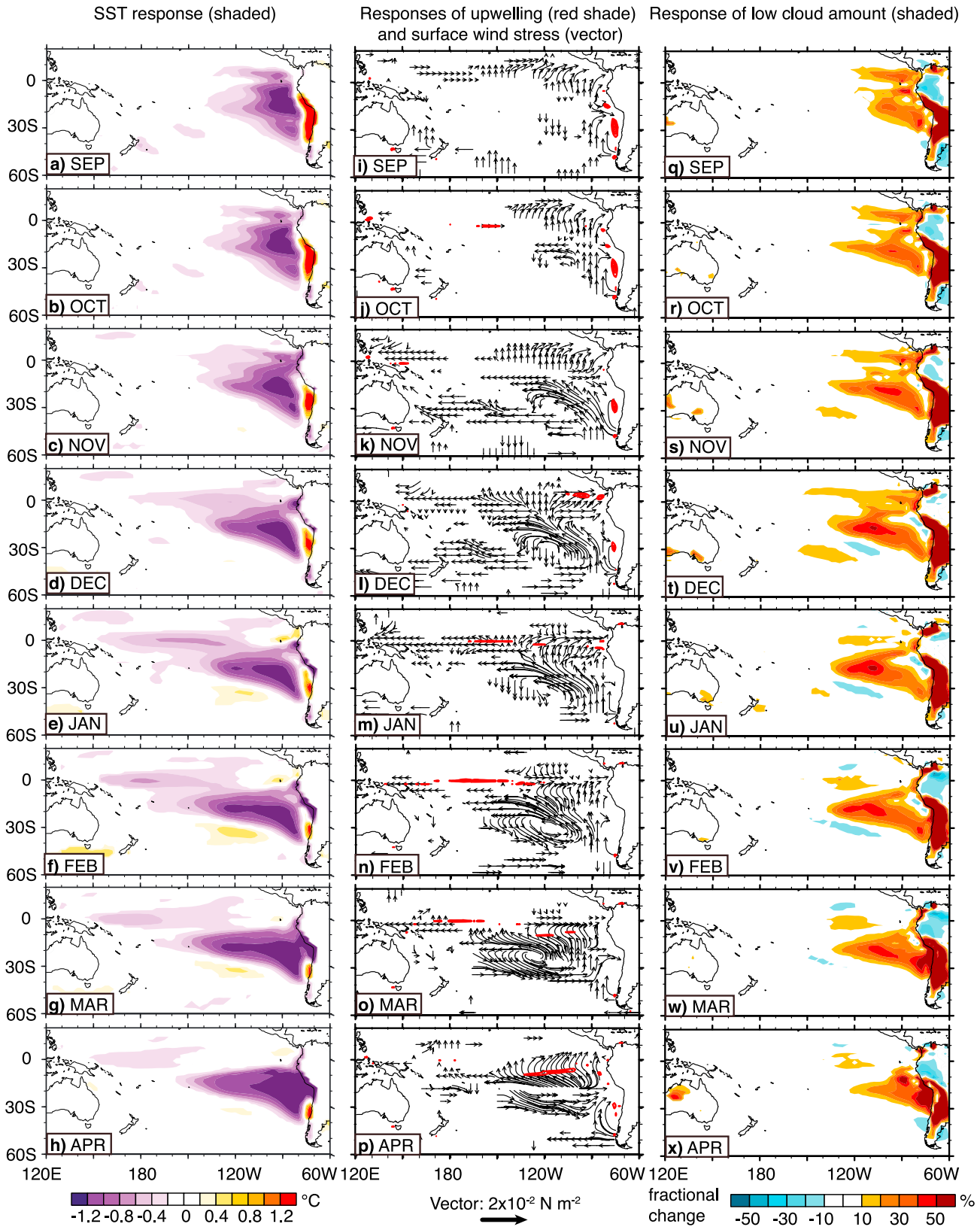

Figure 6. Austral warm season (September to April) monthly differences due to surface uplift (FltAnd − ModAnd) for (a–h) SST (°C, purple shading); (i–p) surface wind stress (vector) and upwelling (red shade: upwelling ≥ 0.2 mm/s averaged across the upper 50 m); and (q–x) percent change in low-cloud cover (%). Responses that passed consistency tests are shown.

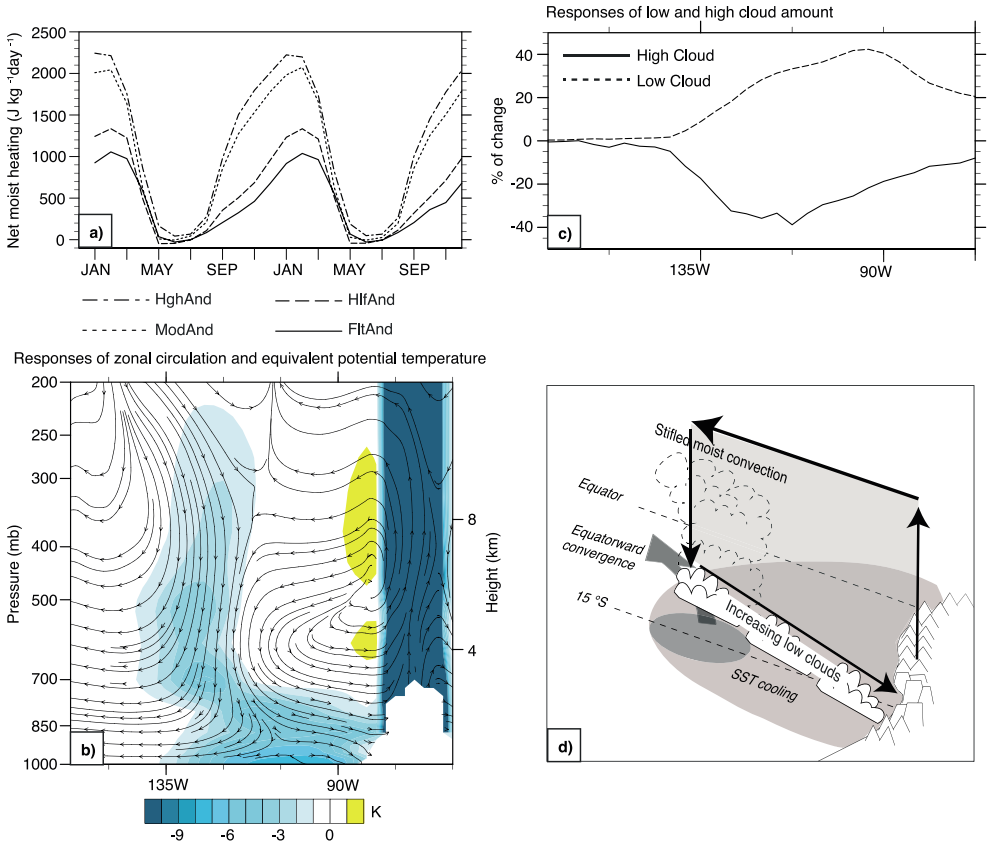

Figure 7. Moist heating and diabatic responses to Andean uplift. (a) Seasonal cycle of the net moist heating (J/kg d^{-1}) over the central Andes (700 hPa, 27.5°S–10.5°S, 82.5°W–57.5°W) for different stages of the Andean uplift. (b) Austral summer (December to February) zonal circulation (streamline) and equivalent potential temperature (K, shaded) differences (ModAnd – FltAnd) in the extraequatorial (10°S–20°S) eastern Pacific. (c) Fractional change (%) in SETP (10°S–20°S) low and high clouds (ModAnd – FltAnd). (d) Schematic diagram summarizing the atmospheric and oceanic responses to enhanced diabatic heating by the Andean uplift during austral summer. Responses shown in Figure 7b have passed the consistency test.

zonal circulation centered at 450 hPa above the eastern extraequatorial Pacific during the austral summer (Figure 7b), which is absent during the wintertime. Similar diabatic responses are reported from atmosphere-only simulations with simplified model physics [*Rodwell and Hoskins*, 2001; *Takahashi and Battisti*, 2007b].

The subsiding branch of the diabatic zonal circulation (shown by streamlines of anomalous flow in Figure 7b) overlies the area of enhanced low-cloud cover (Figures 6t–6v) over the eastern extraequatorial Pacific (10°S–20°S, 90°W–135°W). Subsidence increases the temperature and moisture contrast across the upper boundary layer, providing a stronger cap against deep moist convection. Stifling of cumulus convection is indicated by a reduction of high clouds between 120° and 135°W (Figure 7c) and cooling and drying of the middle tropospheric column 700–250 hPa (Figure 7b). In turn, the reduction in moist convection leads to moisture trapping in the boundary layer and more low clouds (Figure 7c). The linkages between the diabatic circulation, low-cloud cover and moist convection are summarized in Figure 7d.

SST cooling by changes in clouds and convection in the eastern central extraequatorial Pacific (10°S–20°S, 105°W–135°W; Figures 6d–6g) enhances the equatorial-extraequatorial SST gradient during the summertime. This greater SST gradient drives southeasterly winds toward the equator from the Southern Hemisphere (Figure 7d) [*Lindzen and Nigam*, 1987], strengthening the equatorial easterlies.

4. Discussion

4.1. Comparison With Paleoclimatic Changes Since the Late Miocene

Our simulated responses to Andean uplift are consistent with proxy observations from the late Cenozoic. Here we compare in detail the climate response between our HghAnd and HlfAnd simulations, which represent ~2 km

of surface uplift, with proxy records of late Miocene (~13 Ma) and early Pliocene ages (~5 Ma). These simulations were chosen for comparison because they best represent the absolute estimates of paleoelevations [*Insel et al*., 2012]. Similar but slightly smaller responses are found by comparing our FltAnd and ModAnd simulations.

Surface uplift can partially explain SST and thermocline changes documented in proxy records from the northern EEP (6°N, 86°W) and Peruvian coast (16°S, 80°W) (Table 2). Northern EEP upwelling increases by 34% in HghAnd and is consistent with increasing radiolarian species richness since 13 Ma [*LaRiviere et al*., 2012]. Along the northern Peruvian coast, simulated SSTs decrease by ~1.5°C and upwelling increases by ~34%, which compares well with proxy records of cooling of 2.9°C and increases in bioproductivity [*Dekens et al*., 2007]. Andean uplift also produces a zonally asymmetric SST response of ~1°C in the equatorial Pacific, a feature observed in proxy records [*Wara et al*., 2005] but one that is not simulated by CCSM with many other mechanisms that have been hypothesized, including changes in greenhouse gas concentrations [*Lee and Poulsen*, 2006; *Rosenbloom et al*., 2013] and gateways [*Jochum et al*., 2009; *Zhang et al*., 2010]. The equatorial SST asymmetry is crucial for development of a strong Walker circulation capable of sustaining the modern thermocline tilt and ENSO cycle. In this context, the uplift of the Andes may have been contributing to the triggering of the transition from an El Niño-like to modern climate.

The results of our simulations are also consistent with paleoclimate evidence of persistent ENSO activity through the Pliocene [*Watanabe et al*., 2012; *Scroxton et al*., 2011]. Our simulations suggest the possibility that Andean uplift may have changed the frequency and magnitude of El Niño events. At the present time, marine proxy records do not have sufficient length or temporal resolution to evaluate this possibility.

Despite the agreement between our simulations and proxy in several regions, the uplift-induced responses are too small to completely explain past changes in the EEP. Uplift-induced SST cooling, for example, only explains ~20% of the reconstructed signal (Table 2). In addition, thermocline responses are an order of magnitude smaller than those documented by proxies. The major mismatch between proxy and model results occurs along the Central American coast (0°, 82°W). Foraminiferal records suggest strong subsurface cooling and increase of biological productivity at this location (Table 2), which is not captured in our simulations. Uplift-induced responses are also too small to explain the oceanographic changes reported for the western cold tongue (3°N, 118°W) (Table 2), which are attributable to narrowing of the Indonesia [*Rousselle et al*., 2013] and Central American Seaways [*Steph et al*., 2010] through strengthening of the western Pacific warm pool [*Nathan and Leckie*, 2009] and the thermohaline overturning [*Steph et al*., 2010]. Modeling of the climate response to changes in the Indonesian seaways [*Jochum et al*., 2009] and both climate modeling [*Zhang et al*., 2010] and tectonic reconstructions of Central American Seaways [*Montes et al*., 2012] however provide limited support for these hypotheses. Future studies are needed to explain these short-term developments of the Pacific cold tongue system.

4.2. Comparison With Previous Study

Previous studies indicate that uplift-induced surface cooling in the tropical southeastern Pacific is primarily caused by enhanced surface evaporation [*Takahashi and Battisti*, 2007a]. In our experiments, stabilization of the boundary layer by subsidence and horizontal advection plays the dominant role in cooling. This difference likely emerges from different model treatments of boundary layer and low-cloud formation. The intermediate complexity model used by *Takahashi and Battisti* [2007a] does not account for the environmental atmospheric responses to low-cloud formation and boundary layer mixing, which are included in CCSM4 through parameterizations. The more detailed boundary layer representation in CCSM4 reduces drying of the boundary layer induced by large-scale entrainment of tropospheric subsidence, leading to moist conditions and less surface evaporation.

Uplift-induced SST cooling in the SETP is proposed to sustain the meridional and zonal asymmetries of the Intertropical Convergence Zone (ITCZ) in the eastern Pacific [*Takahashi and Battisti*, 2007a, 2007b]. We observe a 10–20% reduction in precipitation in the southern Pacific equatorial region (0–15°S, 150°E–90°W) under high Andes scenarios that is qualitatively consistent with *Takahashi and Battisti* [2007a, 2007b] (>50% reduction) but has a much smaller magnitude. Consequently, in our simulations, the Andean uplift only mildly affects the meridional asymmetry of the ITCZ and South Pacific convergence zone (SPCZ). The uplift mainly affects the zonal asymmetry of the SPCZ during the austral summer through regional diabatic zonal circulation, which pushes the SPCZ westward ~15° (Figure 7b, as indicated by the stifled deep convection).

AGU Paleoceanography

10.1002/2014PA002640

Table 2. Simulated[a] and Reconstructed[b] SST and Thermocline Changes Associated With the Transition From El Niño-Like to Modern Conditions at the Eastern Tropical Pacific Since the Late Miocene

			6°N, 86°W[c, d, e, f]	16°S, 76°W[e] (16°S, 80°W in the Simulation[l])	0°, 95°W[g]	3°S, 91°W[h]	0°, 82°W[c]	1°N, 111°W[j]	3°N, 118°W[k]
Magnitude of SST cooling	Reconstructed		<1°C[c, d], 2°C[f]	2.9°C	~3.8°C from Mg/Ca[g], 2.9°C from U^{k7}_{37}[e]	~5°C	~2°C	5–6°C	~4°C
	Simulated		0.4°C	2.2°C	0.7°C	1.2°C	0.6°C	0.7°C	0.7°C
Thermocline changes	Reconstructed[m]		~6°C subsurface cooling[c], increasing species richness of radiolarian[f, i]	Increasing alkenone mass accumulation rate[e]	~5°C increase of surface-subsurface ocean temperature contrast[g]	Increasing alkenone mass accumulation rate[h], deepwater cooling[f]	~5°C subsurface cooling[c]; increasing opal accumulation rates[d]	NA	Episodic decrease of $\delta^{18}O_{seawater}$ may indicate shoaling of the thermocline at 10–11.5 Ma, 6–6.8 Ma and 4.6–3.6 Ma[j]
	Simulated	Thermocline depth[n]	−2.7 m	−11.3 m	−0.5 m	−0.9 m	+5 m	+0.4 m	+1.5 m
		Upwelling[o]	+36%	+32%	+1%	+2%	−19%	+2%	−5%

[a]Simulated SST and thermocline changes are the consistent differences between HghAnd and HlfAnd averaged over 4°×4° tile centered at the location of the proxy record.
[b]Reconstructed SST and thermocline changes are summarized from the following studies:
[c]*Steph et al.* [2010].
[d]*Groeneveld et al.* [2006].
[e]*Dekens et al.* [2007].
[f]*LaRiviere et al.* [2012].
[g]*Wara et al.* [2005].
[h]*Lawrence et al.* [2006].
[i]*Kamikuri et al.* [2009].
[j]*Zhang et al.* [2014].
[k]*Rousselle et al.* [2013].
[l]The record at the Peru coast (16°S, 76°W) is moved 4° westward due to the underrepresentation of South American coastal line in the model (Figure 1).
[m]Referring to Figure 4a, a 5°C increase of surface-subsurface ocean temperature contrast indicates ~50 m decrease in thermocline depth.
[n]The simulated thermocline depth is defined as the depth of the 20°C isotherm.
[o]The simulated responses of upwelling are reported with values just below the thermocline at 50 m for the first five locations and at 80 m and 100 m for the last two locations due to westward deepening of the equatorial thermocline.

4.3. Model Limitations

Our conclusions concerning the climate response to the uplift of the Andes must be considered in the context of CCSM4's ability to realistically represent the Andean uplift and to reproduce the radiative effect of the tropical low clouds and ENSO cycle. Andean elevations are underrepresented in our CCSM4 configuration. The highest elevation is 3903 m in the HghAnd, which is lower by over 1000 m than the modern peaks surrounding the Bolivia Altiplano. In CCSM4, we find strengthened SST response to the Andean uplift from 1 km to 3 km. This SST response could be greater in a higher-resolution model with more detailed topographic changes. As a result, we consider our estimates to be conservative.

CCSM4 simulates low clouds and ENSO cycle reasonably well. However, low-cloud coverage is still underestimated in subtropical regions worldwide. The net radiative effect of this bias is compensated through a model tuning process to strengthen the cloud radiative forcing [*Nam et al*., 2012]. As a result, the low-cloud bias may not substantially affect our simulated SST responses. The ENSO frequency is quite close to the observations in a modern experiment with CCSM4 [*Deser et al*., 2012], and many atmosphere-ocean feedback crucial to ENSO dynamics are well represented by this model [*Bellenger et al*., 2013, Figure 13]. These results provide confidence that the simulated ENSO response to the Andean uplift is robust. However, CCSM4 still overestimates the overall strength of ENSO [*Deser et al*., 2012] and lacks triggering mechanisms for extremely strong El Niño events [*McPhaden and Yu*, 1999; *Neale et al*., 2008]. Although these biases apply equally in all cases and therefore may not affect the simulated interexperimental responses, it is likely that future advances in ENSO simulation may alter the details of our results.

5. Conclusions

Our simulations provide evidence that the uplift of the Andes dissipates El Niño-like conditions in the eastern tropical Pacific through enhanced low-cloud formation. An increase in low-cloud amounts produces ~2°C cooling in the SETP and ~0.8°C cooling of the equatorial cold tongue region in response to 2 km of uplift starting from a moderate Andean height (~1000 m). This cooling effect is partially attenuated by subthermocline warming due to spin-down of the shallow overturning cell at subtropical southeastern Pacific. Our simulations also provide support that Andean uplift may decrease ENSO frequency and the number of strong El Niño events. These changes result from the increasing variability of zonal wind stress curl north of the equator and the formation of diabatic zonal circulation in response to the Andean uplift during the austral summer.

The simulated response in CCSM4 to Andean uplift can explain some, but not all, of the late Cenozoic changes recorded by marine proxies. Uplift-induced climatic responses can account for ~50% of the reconstructed SST cooling along the Peru coast, strengthening of biological productivity in the northern EEP, and increase in zonal SST and circulation asymmetry across the equatorial Pacific. In summary, our study demonstrates that Andean uplift must be taken into account when considering the long-term evolution of the tropical Pacific.

Acknowledgments

This study was supported by the NSF EAR grants 1019420 and 0907817 to C. Poulsen. We would like to acknowledge the high-performance computing support from Yellowstone (ark:/85065/d7wd3xhc) provided by the NCAR's Computational and Information Systems Laboratory, sponsored by the National Science Foundation. The Yellowstone mass storage system serves the data repository for the simulation data used in this study. These data are available to readers upon request.

References

Alexander, M. A., I. Bladé, M. Newman, J. R. Lanzante, N. C. Lau, and J. D. Scott (2002), The atmospheric bridge: The influence of ENSO teleconnections on air-sea interaction over the global oceans, *J. Clim.*, *15*(16), 2205–2231, doi:10.1175/1520-0442(2002)015<2205:TABTIO>2.0.CO;2.

Bellenger, H., E. Guilyardi, J. Leloup, M. Lengaigne, and J. Vialard (2013), ENSO representation in climate models: From CMIP3 to CMIP5, *Clim. Dyn.*, *42*, doi:10.1007/s00382-013-1783-z.

Bonham, S. G., A. M. Haywood, D. J. Lunt, M. Collins, and U. Salzmann (2009), El Niño–Southern Oscillation, Pliocene climate and equifinality, *Philos. Trans. R. Soc. A*, *367*(1886), 127–156, doi:10.1098/rsta.2008.0212.

Brierley, C. M., A. V. Fedorov, Z. Liu, T. D. Herbert, K. T. Lawrence, and J. P. LaRiviere (2009), Greatly expanded tropical warm pool and weakened hadley circulation in the early Pliocene, *Science*, *323*(5922), 1714–1718, doi:10.1126/science.1167625.

Dekens, P. S., A. C. Ravelo, and M. D. McCarthy (2007), Warm upwelling regions in the Pliocene warm period, *Paleoceanography*, *22*, PA3211, doi:10.1029/2006PA001394.

Deser, C., A. S. Phillips, R. A. Tomas, Y. M. Okumura, M. A. Alexander, A. Capotondi, J. D. Scott, Y.-O. Kwon, and M. Ohba (2012), ENSO and Pacific decadal variability in the community climate system model version 4, *J. Clim.*, *25*(8), 2622–2651, doi:10.1175/JCLI-D-11-00301.1.

Duchon, C. E. (1979), Lanczos filtering in one and two dimensions, *J. Appl. Meteorol.*, *18*(8), 1016–1022, doi:10.1175/1520-0450(1979)018<1016:LFIOAT>2.0.CO;2.

Ehlers, T. A., and C. J. Poulsen (2009), Influence of Andean uplift on climate and paleoaltimetry estimates, *Earth Planet. Sci. Lett.*, *281*(3), 238–248, doi:10.1016/j.epsl.2009.02.026.

Fedorov, A. V., P. S. Dekens, M. McCarthy, A. C. Ravelo, M. Barreiro, R. C. Pacanowski, and S. G. Philander (2006), The Pliocene Paradox (Mechanisms for a Permanent El Nino), *Science*, *312*(5779), 1485–1489, doi:10.1126/science.1122666.

Fedorov, A. V., C. M. Brierley, and K. Emanuel (2010), Tropical cyclones and permanent El Niño in the early Pliocene epoch, *Nature*, *463*(7284), 1066–1070, doi:10.1038/nature08831.

Fedorov, A. V., C. M. Brierley, K. T. Lawrence, Z. Liu, P. S. Dekens, and A. C. Ravelo (2013), Patterns and mechanisms of early Pliocene warmth, *Nature*, *496*(7443), 43–49, doi:10.1038/nature12003.

Galeotti, S., A. von der Heydt, M. Huber, D. Bice, H. Dijkstra, T. Jilbert, L. Lanci, and G. J. Reichart (2010), Evidence for active El Nino Southern Oscillation variability in the Late Miocene greenhouse climate, *Geology*, *38*(5), 419–422, doi:10.1130/G30629.1.

Garzione, C. N., G. D. Hoke, J. C. Libarkin, S. Withers, B. MacFadden, J. Eiler, P. Ghosh, and A. Mulch (2008), Rise of the Andes, *Science*, *320*(5881), 1304–1307, doi:10.1126/science.1148615.

Gent, P. R., S. G. Yeager, R. B. Neale, S. Levis, and D. A. Bailey (2009), Improvements in a half degree atmosphere/land version of the CCSM, *Clim. Dyn.*, *34*(6), 819–833, doi:10.1007/s00382-009-0614-8.

Gent, P. R., G. Danabasoglu, L. J. Donner, M. M. Holland, E. C. Hunke, S. R. Jayne, D. M. Lawrence, R. B. Neale, P. J. Rasch, and M. Vertenstein (2011), The community climate system model version 4, *J. Clim.*, *24*(19), 4973–4991, doi:10.1175/2011JCLI4083.1.

Ghosh, P., C. N. Garzione, and J. M. Eiler (2006), Rapid uplift of the altiplano revealed through ^{13}C-^{18}O bonds in paleosol carbonates, *Science*, *311*(5760), 511–515, doi:10.1126/science.1119365.

Gregory-Wodzicki, K. M. (2000), Uplift history of the Central and Northern Andes: A review, *Geol. Soc. Am. Bull.*, *112*(7), 1091–1105, doi:10.1130/0016-7606(2000)112.

Groeneveld, J., S. Steph, R. Tiedemann, C. Garbe-Schönberg, D. Nürnberg, and A. Sturm (2006), Pliocene mixed-layer oceanography for Site 1241, using combined Mg/Ca and $\delta^{18}O$ analyses of Globigerinoides sacculifer, in *Proceedings of the Ocean Drilling Program: Scientific Results*, vol. 202, pp. 1–27, doi:10.2973/odp.proc.sr.202.209.2006.

Gu, D. (1997), Interdecadal climate fluctuations that depend on exchanges between the tropics and extratropics, *Science*, *275*(5301), 805–807, doi:10.1126/science.275.5301.805.

Haug, G. H., and R. Tiedemann (1998), Effect of the formation of the Isthmus of Panama on Atlantic Ocean thermohaline circulation, *Nature*, *393*(6686), 673–676, doi:10.1038/31447.

Haywood, A. M., P. J. Valdes, and V. L. Peck (2007), A permanent El Niño-like state during the Pliocene?, *Paleoceanography*, *22*, PA1213, doi:10.1029/2006PA001323.

Insel, N., C. J. Poulsen, and T. A. Ehlers (2010), Influence of the Andes on South American moisture transport, convection, and precipitation, *Clim. Dyn.*, *35*(7–8), 1477–1492, doi:10.1007/s00382-009-0637-1.

Insel, N., C. J. Poulsen, T. A. Ehlers, and C. Sturm (2012), Response of meteoric $\delta^{18}O$ to surface uplift — Implications for Cenozoic Andean Plateau growth, *Earth Planet. Sci. Lett.*, *317-318*, 262–272, doi:10.1016/j.epsl.2011.11.039.

Jochum, M., B. Fox Kemper, P. H. Molnar, and C. Shields (2009), Differences in the Indonesian seaway in a coupled climate model and their relevance to Pliocene climate and El Niño, *Paleoceanography*, *24*, PA1212, doi:10.1029/2008PA001678.

Kamikuri, S.-I., I. Motoyama, H. Nishi, and M. Iwai (2009), Evolution of Eastern Pacific Warm Pool and upwelling processes since the middle Miocene based on analysis of radiolarian assemblages: Response to Indonesian and Central American Seaways, *Palaeogeogr. Palaeoclimatol. Palaeoecol.*, *280*(3–4), 469–479, doi:10.1016/j.palaeo.2009.06.034.

Kirtman, B. P. (1997), Oceanic Rossby wave dynamics and the ENSO period in a coupled model, *J. Clim.*, *10*(7), 1690–1704, doi:10.1175/1520-0442(1997)010<1690:ORWDAT>2.0.CO;2.

Klinger, B. A., J. P. McCreary Jr., and R. Kleeman (2002), The relationship between oscillating subtropical wind stress and equatorial temperature*, *J. Phys. Oceanogr.*, *32*(5), 1507–1521, doi:10.1175/1520-0485(2002)032<1507:TRBOSW>2.0.CO;2.

LaRiviere, J. P., A. C. Ravelo, A. Crimmins, P. S. Dekens, H. L. Ford, M. Lyle, and M. W. Wara (2012), Late Miocene decoupling of oceanic warmth and atmospheric carbon dioxide forcing, *Nature*, *486*(7401), 97–100, doi:10.1038/nature11200.

Lawrence, K. T., Z. Liu, and T. D. Herbert (2006), Evolution of the Eastern Tropical Pacific Through Plio-Pleistocene Glaciation, *Science*, *312*(5770), 79–83, doi:10.1126/science.1120395.

Lee, S.-Y., and C. J. Poulsen (2006), Sea ice control of Plio–Pleistocene tropical Pacific climate evolution, *Earth Planet. Sci. Lett.*, *248*(1–2), 253–262, doi:10.1016/j.epsl.2006.05.030.

Leier, A., N. McQuarrie, C. Garzione, and J. Eiler (2013), Stable isotope evidence for multiple pulses of rapid surface uplift in the Central Andes, Bolivia, *Earth Planet. Sci. Lett.*, *371–372*, 49–58, doi:10.1016/j.epsl.2013.04.025.

Lenters, J. D., and K. H. Cook (1997), On the origin of the Bolivian High and related circulation features of the South American climate, *J. Atmos. Sci.*, *54*, 656–677.

Lindzen, R. S., and S. Nigam (1987), On the role of sea surface temperature gradients in forcing low-level winds and convergence in the tropics, *J. Atmos. Sci.*, *44*(17), 2418–2436, doi:10.1175/1520-0469(1987)044<2418:OTROSS>2.0.CO;2.

McPhaden, M. J., and X. Yu (1999), Equatorial waves and the 1997-98 El Niño, *Geophys. Res. Lett.*, *26*(19), 2961–2964, doi:10.1029/1999GL004901.

Molnar, P., and M. A. Cane (2007), Early Pliocene (pre–Ice Age) El Niño–like global climate: Which El Niño?, *Geosphere*, *3*(5), 337, doi:10.1130/GES00103.1.

Montes, C., G. Bayona, A. Cardona, D. M. Buchs, C. A. Silva, S. Morón, N. Hoyos, D. A. Ramírez, C. A. Jaramillo, and V. Valencia (2012), Arc-continent collision and orocline formation: Closing of the Central American seaway, *J. Geophys. Res.*, *117*, B04105, doi:10.1029/2011JB008959.

Nam, C., S. Bony, J. L. Dufresne, and H. Chepfer (2012), The "too few, too bright"tropical low-cloud problem in CMIP5 models, *Geophys. Res. Lett.*, *39*, L21801, doi:10.1029/2012GL053421.

Nathan, S. A., and R. M. Leckie (2009), Early history of the Western Pacific Warm Pool during the middle to late Miocene (~13.2–5.8 Ma): Role of sea-level change and implications for equatorial circulation, *Palaeogeogr. Palaeoclimatol. Palaeoecol.*, *274*(3), 140–159, doi:10.1016/j.palaeo.2009.01.007.

Neale, R. B., J. H. Richter, and M. Jochum (2008), The impact of convection on ENSO: From a delayed oscillator to a series of events, *J. Clim.*, *21*(22), 5904–5924, doi:10.1175/2008JCLI2244.1.

Poulsen, C. J., T. A. Ehlers, and N. Insel (2010), Onset of convective rainfall during gradual late miocene rise of the central andes, *Science*, *328*(5977), 490–493, doi:10.1126/science.1185078.

Rodwell, M. J., and B. J. Hoskins (2001), Subtropical anticyclones and summer monsoons, *J. Clim.*, *14*(15), 3192–3211, doi:10.1175/1520-0442(2001)014<3192:SAASM>2.0.CO;2.

Rosenbloom, N. A., B. L. Otto-Bliesner, E. C. Brady, and P. J. Lawrence (2013), Simulating the mid-Pliocene warm period with the CCSM4 model, *Geosci. Model Dev.*, *6*(2), 549–561, doi:10.5194/gmd-6-549-2013.

Rousselle, G., C. Beltran, M. A. Sicre, I. Raffi, and M. De Rafelis (2013), Changes in sea-surface conditions in the Equatorial Pacific during the middle Miocene–Pliocene as inferred from coccolith geochemistry, *Earth Planet. Sci. Lett.*, *361*, 412–421, doi:10.1016/j.epsl.2012.11.003.

Scroxton, N., S. G. Bonham, R. Rickaby, S. Lawrence, M. Hermoso, and A. M. Haywood (2011), Persistent El Niño–Southern Oscillation variation during the Pliocene Epoch, *Paleoceanography*, *26*, PA2215, doi:10.1029/2010PA002097.

Steph, S., R. Tiedemann, M. Prange, J. Groeneveld, M. Schulz, A. Timmermann, D. Nürnberg, C. Rühlemann, C. Saukel, and G. H. Haug (2010), Early Pliocene increase in thermohaline overturning: A precondition for the development of the modern equatorial Pacific cold tongue, *Paleoceanography*, *25*, PA2202, doi:10.1029/2008PA001645.

Takahashi, K., and D. S. Battisti (2007a), Processes Controlling the Mean Tropical Pacific Precipitation Pattern. Part I: The Andes and the Eastern Pacific ITCZ, *J. Clim.*, *20*(14), 3434–3451, doi:10.1175/JCLI4198.1.

Takahashi, K., and D. S. Battisti (2007b), Processes Controlling the Mean Tropical Pacific Precipitation Pattern. Part II: The SPCZ and the Southeast Pacific Dry Zone, *J. Clim.*, *20*(23), 5696–5706, doi:10.1175/2007JCLI1656.1.

Trenberth, K. E. (1997), The definition of El Niño, *Bull. Am. Meteorol. Soc.*, *78*(12), 2771–2777, doi:10.1175/1520-0477(1997)078<2771:TDOENO>2.0.CO;2.

Vecchi, G. A., and B. J. Soden (2007), Global warming and the weakening of the tropical circulation, *J. Clim.*, *20*(17), 4316–4340, doi:10.1175/JCLI4258.1.

Wara, M. W., A. C. Ravelo, and M. L. Delaney (2005), Permanent El Nino-Like Conditions During the Pliocene Warm Period, *Science*, *309*(5735), 758–761, doi:10.1126/science.1112596.

Watanabe, T., et al. (2012), Permanent El Niño during the Pliocene warm period not supported by coral evidence, *Nature*, *471*(7337), 209–211, doi:10.1038/nature09777.

Wood, R., and C. S. Bretherton (2004), Boundary layer depth, entrainment, and decoupling in the cloud-capped subtropical and tropical marine boundary layer, *J. Clim.*, *17*, 3576–3588, doi:10.1175/1520-0442(2004)017<3576:BLDEAD>2.0.CO;2.

Xu, H., Y. Wang, and S.-P. Xie (2004), Effects of the andes on eastern pacific climate: A regional atmospheric model study*, *J. Clim.*, *17*, 589–602, doi:10.1175/1520-0442(2004)017<0589:EOTAOE>2.0.CO;2.

Zhang, X., et al. (2010), Changes in equatorial Pacific thermocline depth in response to Panamanian seaway closure: Insights from a multi-model study, *Earth Planet. Sci. Lett.*, *317-318*, 76–84, doi:10.1016/j.epsl.2011.11.028.

Zhang, Y. G., M. Pagani, and Z. Liu (2014), A 12-million-year temperature history for the Tropical Pacific Ocean, *Science*, *344*(6179), 84–87, doi:10.1126/science.1246172.